

An inhomogeneous model for the Galactic halo: a possible explanation for the spread observed in s- and r-process elements

G. Cescutti ^{*}

Dipartimento di Astronomia, Università di Trieste, via G.B. Tiepolo 11, I-34131

Received xxxx / Accepted xxxx

ABSTRACT

Aims. We propose an explanation for the considerable scatter of the abundances of neutron capture elements observed in low-metallicity stars in the solar vicinity, compared to the small star-to-star scatter observed for the α -elements.

Methods. We have developed a stochastic chemical evolution model in which the main assumption is a random formation of new stars subject to the condition that the cumulative mass distribution follows a given initial mass function.

Results. With our model, we are able to reproduce the different spreads of neutron capture elements and α -elements in low-metallicity stars.

Conclusions. The reason for different observed spread in neutron capture elements and α -elements resides in the random birth of stars, coupled with different stellar mass ranges, from which α -elements and neutron capture elements originate. In particular, the site of production of α -elements is the whole range of massive stars, from 10 to $80M_{\odot}$ whereas the mass range of production for neutron capture elements lies between 12 and $30M_{\odot}$.

Key words. Galaxy: halo - Galaxy: evolution - Stars: abundances - nuclear reactions, nucleosynthesis, abundances

1. Introduction

Early work by Gilroy et al. (1988) first proposed that the stellar abundances of very heavy elements with respect to iron, particularly [Eu/Fe], show a large scatter at low metallicities. Their work suggested that this scatter appears to diminish with increasing metallicity. This was confirmed by the large spread observed later on in the [Ba/Fe] and [Eu/Fe] ratios in halo stars (e.g., McWilliam et al. 1995; Ryan et al. 1996). A more extensive study by Burris et al. (2000) confirmed the very large star-to-star scatter in the early Galaxy, while studies of stars at higher metallicities, involving mostly disk stars (Edvardsson et al. 1993; Woolf, Tomkin, & Lambert 1995), show little scatter. In the last few years, a great deal of observational work on galactic stars appeared: Fulbright (2000); Mashonkina & Gehren (2000, 2001); Koch & Edvardsson (2002); Honda et al. (2004); and Ishimaru et al. (2004). All these works confirmed the presence of the spread for these elements and this spread can reach 2 dex at [Fe/H]¹ ~ -3 . It is worth noting that such a high spread is not found for the [α /Fe] ratios in very metal-poor stars (down to [Fe/H] = -4.0, Cayrel et al. 2004); in fact, the spread for these elements is around 0.5 dex at low metallicities. This fact suggests that the spread, if real, is a characteristic of these heavy elements and not only due to an inhomogeneous

mixing in the early halo phases, as suggested by several authors (Tsujimoto et al. 1999; Ishimaru & Wanajo 1999).

Recently, several studies have attempted to follow the enrichment history of the Galactic halo with special emphasis given to the gas dynamical processes occurring in the early Galaxy: Tsujimoto, Shigeyama, & Yoshii (1999) provided an explanation for the spread of Eu observed in the oldest halo stars in the context of a model of supernova-induced star formation; Ikuta & Arimoto (1999) and McWilliam & Searle (1999) studied the metal enrichment of the Galactic halo with the help of a stochastic model aimed at reproducing the observed Sr abundances; Raiteri et al. (1999) followed the Galactic evolution of Ba by means of a hydrodynamical N-body/smoothed particle hydrodynamics code; and Argast et al. (2000) concentrated on the effects of local inhomogeneities in the Galactic halo produced by individual supernova (SN) events, accounting in this way for the observed scatter of some (but not all) elements typically produced by type II SNe. Besides a spread for r-process elements, they also predicted a spread of more than 2 dex for Mg and O at [Fe/H] = -3, which is too large compared to the observational data. Finally, Travaglio et al. (2004) investigated whether incomplete mixing of gas in the Galactic halo can lead to local chemical inhomogeneities in the interstellar medium (ISM) involving heavy elements, in particular Eu, Ba, and Sr. They reproduced the spread for these elements, but left unexplained why the spread is present only for neutron capture elements whereas it is much smaller for the other elements (for

^{*} email to: cescutti@oats.inaf.it

¹ We adopt the usual spectroscopic notations that [A/B] = $\log_{10}(N_A/N_B)_{\star} - \log_{10}(N_A/N_B)_{\odot}$ and that $\log \epsilon(A) = \log_{10}(N_A/N_H) + 12.0$, for elements A and B

example α -elements). Concerning the α -elements, Argast et al. (2002) and Karlsson & Gustafsson (2005) attempted to explain the small dispersion in these elements from two different points of view: a different iron yield distribution as a function of progenitor mass for Argast et al. (2002), and cosmic selection effects favoring contributions from supernovae in a certain mass range for Karlsson & Gustafsson (2005).

The purpose of this paper is to explain the different spread observed in the halo stars for different elements. Cescutti et al. (2006) have suggested the best stellar yields to fit the trend of the mean abundances for Eu and Ba in the framework of a homogeneous chemical evolution model (Chiappini et al. 1997, 2001). In the present paper, using the same yields of Cescutti et al. (2006), we show the results of a stochastic chemical evolution model that we have developed to explain the different observed spreads for different elements in the halo stars. The paper is organized as follows: in Sect. 2 we present the observational data; in Sect. 3 the inhomogeneous chemical evolution model is presented; and in Sect. 4 the adopted nucleosynthesis prescriptions are described. In Sect. 5 we present the results; and in Sect. 6 some conclusions are drawn.

2. Observational data

For the extremely metal-poor stars ($-4 < [\text{Fe}/\text{H}] < -3$), we adopted the recent results from UVES Large Program "First Star" (Cayrel et al. 2004, François et al. 2007). For the abundances in the remaining range of $[\text{Fe}/\text{H}]$, we took high quality data of various sources published in the literature. These are summarized in Table 1. We homogenized all of these data by normalizing them to the solar abundances by Asplund et al. (2005).

3. Inhomogeneous chemical evolution model for the Milky Way halo

For comparison with a homogeneous chemical evolution model, we choose to use the same parameters of the chemical evolution (star formation rate, initial mass function, stellar lifetime, nucleosynthesis, gas density threshold) as those of the homogeneous model used in Cescutti et al. (2006). For this reason, we model the chemical evolution of the halo of the Milky Way for the duration of 1 Gyr. We consider that the halo consists of many independent cubic regions, each with the same typical volume, and each region does not interact with the others. We decided to have a typical volume of $2.8 \cdot 10^6 \text{ pc}^3$, in this way the surface of the volume, taken as the side of a cube, is $2 \cdot 10^4 \text{ pc}^2$. The number of assumed volumes is 100. In order to ensure good statistical results, we test that a larger number of volumes and found that the statistics do not significantly change, but the model is slowed down. The dimension of the volume is large enough to allow us to neglect the interaction among different volumes, at least as a first approximation. In fact, for typical ISM densities, a supernova remnant becomes indistinguishable from the ISM – i.e., merges with the ISM – before reaching $\sim 50 \text{ pc}$ (Thornton et al. 1998), less than the size of our cubic region. We do not use larger volumes because we would lose the stochasticity we are looking for; in fact, as we tested for

increasing volumes, the model tends to be homogeneous. We use timesteps of 1 Myr, which is an interval of time shorter than any stellar lifetime considered here; in fact, the maximum stellar mass considered here is $80 M_\odot$ with a lifetime of $\sim 3 \text{ Myr}$. At the same time, this timestep is longer than the cooling time of the SN bubbles, which is normally $\sim 0.1\text{--}0.2 \text{ Myr}$ and at maximum 0.8 Myr . We describe later in this same Sect. how we calculate this cooling time. With this timestep we can say, in first approximation, that an homogenous mixing takes place and, at least for the first period, only a few stars pollute the ISM; this is again important from the point of view of the stochasticity of the model.

In each region, we assume the same law for the infall of the gas with primordial composition; originally, in the homogeneous model, we have this law for the halo phase:

$$\frac{d\sigma_{\text{tot}}(t)}{dt} = I_{\text{nfall}}^\sigma e^{-t/\tau} \quad (1)$$

where the parameter I_{nfall}^σ is equal to $16 M_\odot \text{ Gyr}^{-1} \text{ pc}^{-2}$, and this law is a function of surface gas density. However, we want to use this law for our box, and so considering the side of the cube ($2 \cdot 10^4 \text{ pc}^2$) as the typical surface we obtain in each volume, multiplying the previous equation by this typical surface:

$$\frac{dM_{\text{tot}}^{\text{Vol}}(t)}{dt} = I_{\text{nfall}}^{\text{Vol}} e^{-t/\tau} \quad (2)$$

where $I_{\text{nfall}}^{\text{Vol}}$ is $320 M_\odot \text{ Myr}^{-1}$; τ is in both cases 1 Gyr. We consider a threshold in the gas surface density, which means that below this threshold the star formation is blocked, due to the insufficient gas density in the system. The value of this gas surface density threshold is $\sigma_{\text{threshold}} = 4 M_\odot \text{ pc}^{-2}$, as in the homogeneous model, so with the surface we consider, it becomes in each volume $M_{\text{threshold}} = 80 \cdot 10^3 M_\odot$. The star formation rate $\psi(t)$ is defined:

$$\psi(t) = \nu \left(\frac{M_{\text{gas}}(t)}{M_{\text{threshold}}} \right)^{1.5} \quad (3)$$

where $M_{\text{gas}}(t)$ is the gas mass inside the considered box and the parameter ν is $80 M_\odot \text{ Myr}^{-1}$; this parameter is set to match the star formation rate of the homogenous model during the halo phase. So, when the gas density threshold is reached for the first time, the mass that is transformed into stars in a timestep (hereafter, $M_{\text{stars}}^{\text{new}}$) is $80 M_\odot$. In this way, we note that the code can form at any timestep stars of any mass up to the considered maximum stellar mass (i.e. $80 M_\odot$), and the code can form all the stellar masses up to $80 M_\odot$. So, with the considered surface (with the considered gas density threshold), we are also overcoming the risk of having a bias toward low mass stars, when the code randomly chooses the masses of the forming stars.

Knowing the $M_{\text{stars}}^{\text{new}}$, we assign the mass to one star with a random function, weighted according to the initial mass function (IMF) of Scalo (1986) in the range between 0.1 and $80 M_\odot$. Then we extract the mass of another star and we repeat this cycle until the total mass of newly-formed stars exceeds $M_{\text{stars}}^{\text{new}}$. In this way, in each region, at each timestep, the $M_{\text{stars}}^{\text{new}}$ is the same but the total number and mass distribution of the stars

Table 1. The authors from which we adopt the observational data for each considered element.

	Eu	Ba	La	Sr	Y	Zr	Ca	Mg	Si
Burris et al. (2000)	X	X		X	X	X			
Carney et al. (1997)							X	X	X
Carretta et al. (2002)							X	X	X
Cayrel et al. (2004)							X	X	X
Cowan et al. (2005)	X		X			X			
Edvardsson et al. (1993)		X			X	X	X	X	X
François et al. (2007)	X	X	X	X	X	X			
Fulbright (2000)	X	X			X	X	X	X	X
Fulbright (2002)	X	X			X	X	X	X	X
Gilroy et al. (1998)	X	X	X	X	X	X			
Gratton & Sneden (1988)		X		X	X				
Gratton & Sneden (1994)	X	X	X	X	X	X			
Honda et al. (2004)	X	X	X	X	X	X	X	X	X
Ishimaru et al. (2004)	X	X		X					
Johnson (2002)	X	X	X	X	X	X	X	X	X
Koch & Edvardsson (2002)	X								
Mashonkina & Gehren (2000, 2001)	X	X		X					
McWilliam et al. (1995)	X	X	X	X	X	X	X	X	X
McWilliam & Rich (1994)	X	X	X		X	X	X	X	X
Nissen & Schuster (1997)		X			X				
Pompeia et al. (2003)			X						
Prochaska et al. (2000)	X	X			X		X	X	X
Ryan et al. (1991)	X	X		X	X		X	X	X
Ryan et al. (1996)	X	X		X	X	X	X	X	X
Stephens (1999)		X			X		X	X	X
Stephens & Boesgaard (2002)		X			X		X	X	X

are different, and we know the mass of each star contained in each region, when it is born and when it will die, assuming the stellar lifetimes of Maeder & Meynet (1989). We compute the chemical evolution in the following way: at the end of its lifetime, each star enriches the interstellar medium with newly-produced elements (see the next Sect.) as a function of its mass and metallicity. The total mass of each element is determined at the end of the lifetime of each star, taking into account the enrichment due to that star and due to the already present mass of each element locked in that star when it is born. The model does not take into account the pollution produced by stars with mass $< 3M_{\odot}$ because their lifetimes exceed the duration of the simulation. The existence of SNe Ia is also taken into account, according to the prescriptions of Matteucci & Greggio (1986), in the single degenerate scenario. We consider that a fraction of the stellar masses in the range $3-16M_{\odot}$ would be binary systems which can produce SN Ia. The correct number of observed SN Ia at the present time (see Cappellaro et al. 1999) is reproduced if this percentage is 5% and we evaluate, again using a random extraction, if the system is a progenitor of a SN Ia. We also determine the mass of the secondary through the distribution function:

$$f(\mu) = 2^{1+\gamma}(1+\gamma)\mu^{\gamma} \quad (4)$$

with $\gamma = 2$, where μ is the fraction of the mass of the secondary star to the total mass of the system and in this way we know when the SN Ia will explode; in fact, its lifetime is that of the secondary star of the binary system. In Fig. 1, the SNe Ia rate

is compared to the SNe II rate. Due to the threshold in the gas density that we impose, the star formation starts only after 250 Myr and, at this stage, the first SNe II start to explode. With a time delay of about 30 Myr, the first SNe Ia take place. In our model we consider the single degenerate scenario and 30 Myr is the shortest timescale for a SN Ia to explode, being the lifetime of the most massive progenitor leading to the formation of a C-O white dwarf (i.e. a star of $8M_{\odot}$). We stop the star formation at 1 Gyr and the SNe II rate falls abruptly to zero, correctly, the largest lifetime of a SNII being 30 Myr, whereas the SNe Ia continue to explode, the lifetime of the progenitors of a SN Ia being as long as 10 Gyr.

We assume that the ejecta produced by the dying stars mix with the surrounding ISM only after these ejecta cool down significantly. The cooling timescale of the ejecta is calculated as follows:

$$t_{cooling} = \frac{3kT}{n\Lambda(T, z)} \quad (5)$$

where n , T , and z are the average number density, the temperature, and the metallicity in the cubic region, respectively. $\Lambda(T, z)$ is the cooling function, taken from Sutherland & Dopita (1993). We know the total gas mass and the thermal energy (assuming 10^{51} erg of energy after each SN explosion), therefore in each cubic region, at each timestep, we can calculate n and T . The resulting cooling timescales are normally $\sim 0.1-0.2$ Myr and reach at maximum 0.8 Myr in a set of 100 volumes. Since the cooling timescales are always smaller than the timestep of our simulation (1 Myr), we decided to neglect this delay time,

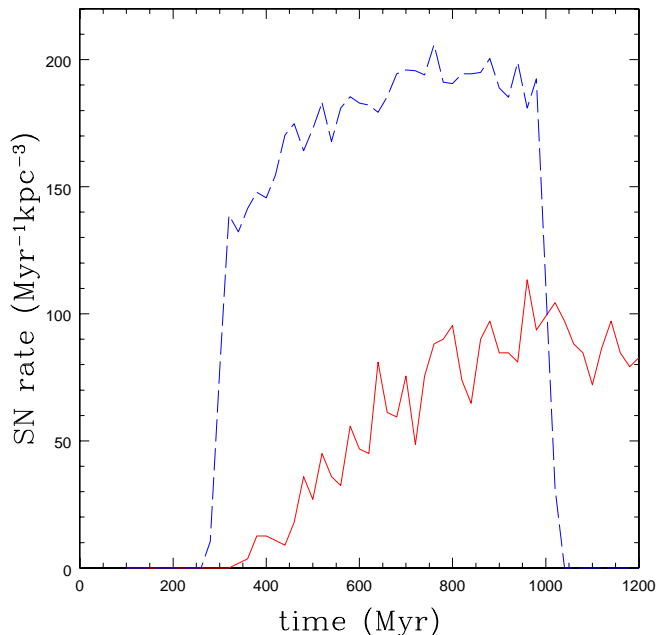


Fig. 1. The SNIa rate (solid line) and SNII rate (dashed line) in the halo. Note that the rate of SNIa is multiplied by ten.

so that the mixing in each simulated cubic volume is instantaneous. The model follows the chemical evolution of 10 elements (Si, Ca, Mg, Fe, Sr, Y, Zr, Ba, La and Eu) in each region. If the model is correct, our predictions will approximate the results of the homogeneous model, having the same parameters, as the number of stars increases. On the other hand, our model shows the spread of chemical enrichment at low metallicity that can be produced by different stars of various masses, where the number of stars is low and the random effects in the birth of stellar masses are important.

4. Nucleosynthesis Prescriptions

For the nucleosynthesis prescriptions of the Fe, Si, Ca, and Mg, we adopted those suggested by François et al. (2004) both for single stars and SNeIa. They started with the Woosley & Weaver (1995) yields for massive stars at the solar composition, metallicity independent; they use the Iwamoto et al. (1999) yields for type Ia SNe. Then, they compared the model results with observational data with the aim of imposing constraints upon stellar yields. To best fit the data in the solar neighborhood, they modified the original yields by Woosley & Weaver (1995) and by Iwamoto et al. (1999). In particular, they changed Mg by increasing in stars with masses from 11 to 20 M_{\odot} and decreasing in masses larger than 20 M_{\odot} . The Mg yield has also been increased in SNeIa. The Si yields have increased slightly in stars above 40 M_{\odot} . Ca and Fe (the solar abundance case) in massive stars from Woosley & Weaver (1995) are the best to fit the abundance patterns of these elements since they do not need any changes. We underline that the site of production of α -elements is the whole range of massive stars. For Fe, the main producers are SNeIa, but a fraction arises also from

the whole range of massive stars. For the nucleosynthesis prescriptions of the r-process contribution, we used those of model 1 for Ba and Eu (see Cescutti et al. 2006), and the results of Cescutti et al. (2007a) for La. For Sr, Y, and Zr we used the results shown in Cescutti (2007b). We have assumed that these neutron capture elements are produced by r-process in massive stars, but only in the mass range 12-30 M_{\odot} . These empirical yields have been chosen to reproduce the surface abundances for all these neutron capture elements in low-metallicity stars as well as the Sr, Y, Zr, Ba, Eu, and La solar abundances, taking in account the s-process contribution at high metallicities by means of the yields of Busso et al. (2001) for La and Ba and those of Travaglio et al. (2004) for Sr, Y, and Zr in the mass range 1.5-3 M_{\odot} . Eu is considered to be a purely r-process element produced in the same range of masses. This choice is extensively discussed in Cescutti et al. (2006) and the nucleosynthesis prescriptions of the r-process contribution are summarized in Table 2. In this model, we do not take into account the s-process contribution for these elements because its enrichment timescale exceeds the duration of the simulation, this process taking place in low mass stars (1.5-3 M_{\odot}).

5. Results

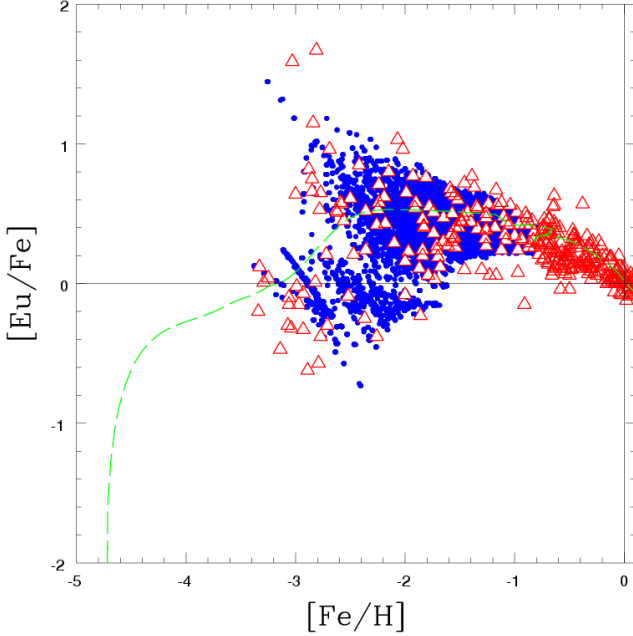
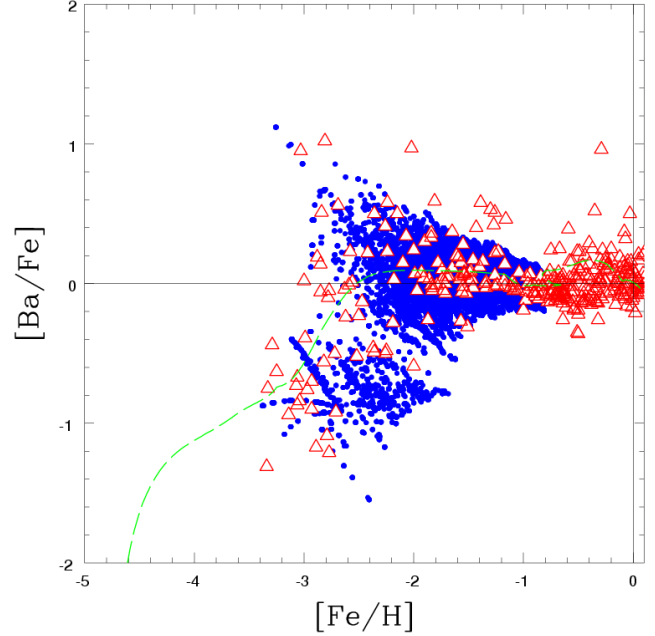
5.1. The ratios of α -elements and neutron capture elements to Fe

We discuss here the results of our simulations compared to the observational data and to the prediction of the homogeneous model of Cescutti et al. (2006). We show the [Eu/Fe], [Ba/Fe], [La/Fe], [Sr/Fe], [Y/Fe], and [Zr/Fe] ratios as functions of [Fe/H] in the Figs. 2, 3, 4, 5, 6, and 7, respectively; for α -elements we show [Si/Fe], [Ca/Fe], and [Mg/Fe] as functions of [Fe/H] in Figs. 8, 9, and 10, respectively. In these Figs., we show the simulated living stars at the present time (blue points) together with the observations (red triangles).

It is worth noting that our model reproduces the large spread observed in the abundances of metal-poor stars for the neutron capture elements and, at the same time, the small spread for the α -elements. The chemical enrichment observed in very metal-poor stars is due only to nucleosynthesis in massive stars. The site of production of the α -elements is different than the one of neutron capture elements (as described in the previous Sect.): the α -elements and Fe are produced in the whole range of massive stars (10-80 M_{\odot}); on the other hand, the neutron capture elements are assumed to be produced in the smaller range between 12 and 30 M_{\odot} . Therefore, in regions biased randomly toward stars less massive than 30 M_{\odot} , the ratio of neutron capture elements over Fe is high. The opposite happens in regions where a large fraction of the stars are more massive than 30 M_{\odot} . This fact produces, in our inhomogeneous model, a large spread for the rates of neutron capture elements to Fe, but not for the ratio of the α -elements to Fe, since the α -elements and Fe are produced in the same range. The idea of a small range of the r-elements progenitors, as an explanation of the large scatter, having been previously proposed by Ishimaru & Wanajo (1999) and Argast et al. (2000) (although with different mass ranges and mass dependences of

Table 2. The used prescriptions of the mass fractions of newly-produced elements for neutron capture elements in massive stars (r-process).

M_{star}	X_{Ba}^{new}	X_{Eu}^{new}	X_{La}^{new}	X_{Sr}^{new}	X_{Y}^{new}	X_{Zr}^{new}
12.	$9.00 \cdot 10^{-7}$	$4.50 \cdot 10^{-8}$	$9.00 \cdot 10^{-8}$	$1.80 \cdot 10^{-6}$	$3.60 \cdot 10^{-7}$	$1.80 \cdot 10^{-6}$
15.	$3.00 \cdot 10^{-8}$	$3.00 \cdot 10^{-9}$	$3.00 \cdot 10^{-9}$	$7.50 \cdot 10^{-8}$	$2.10 \cdot 10^{-8}$	$1.65 \cdot 10^{-7}$
30.	$1.00 \cdot 10^{-9}$	$5.00 \cdot 10^{-10}$	$1.00 \cdot 10^{-10}$	$3.25 \cdot 10^{-9}$	$1.00 \cdot 10^{-9}$	$5.00 \cdot 10^{-9}$

**Fig. 2.** [Eu/Fe] vs [Fe/H]. The abundances of simulated living stars at the present time are indicated by the blue dots. The red triangles are the observational data from various authors (see Table 1) The dashed line is the prediction of the homogeneous model (Cescutti et al. 2006, model 1).**Fig. 3.** As in Fig. 2, but for [Ba/Fe]. The authors of the observational data are listed in Table 1. The dashed line is the prediction of the homogeneous model (Cescutti et al. 2006, model 1).

the yields). Nevertheless, Ishimaru & Wanajo (1999) do not show results for α -elements; Argast et al. (2000) show results for α -elements, but the resulting spread of their model is too large compared to the observed one. We have to emphasize that if we use, the original yields by Woosley & Weaver, rather than the yields by François et al. (2004), our model also shows a larger spread than the observed spread for the Mg (but not in the case of Ca). This is due to the strong dependence, in the original work of Woosley & Weaver, of the Mg yields on stellar mass, compared to the smaller dependence on the progenitor mass in the work of François et al. (2004). However, we think that it is reasonable to use the yields of François et al. (2004) for Mg, since recently many nuclear reaction data have changed, in particular in the case of this element. More recent nucleosynthesis yields, such as that found by Nomoto et al. (2006), show a smaller dependence on the progenitor mass as well. In the Figs. 11 and 12, we show the relative frequency of stars at a given [El/Fe] ratio for different enrichment phases. To do that, we have used only the stars still alive in the halo, namely those with a mass $< 0.8M_{\odot}$. The different enrichment

phases: $[Fe/H] < -2$ and $-2 < [Fe/H] < -1$ are given in the panels from top to bottom for Si and Eu. In these Figs., the solid lines are the predictions of the model and the dashed lines are the observational data.

At low metallicity, the model predicts a quite narrow distribution for Si, whereas for Eu the distribution of the stars is broad, in agreement with the observations. At higher metallicities, both elements have predicted distributions slightly narrower than the observed ones. Nevertheless, we emphasize that the measured ratios are affected by observational errors, which in general are of the order 0.1 dex and could be responsible for the broader distributions of the observational data. In the low metallicity range, we noticed some discrepancies. For instance, the observed distribution of [Si/Fe] is slightly broader than the predicted distribution; therefore, a more careful analysis of nucleosynthesis yields may be required (for instance, using metallicity dependent Si yields). The model is not able to reproduce ultra metal-poor stars, whereas stars with these metallicity are observed. In particular, the model predicts the formation of some metal free stars at the beginning, but then the metallicity jumps to $[Fe/H] \sim -3.6$. This may be due to an

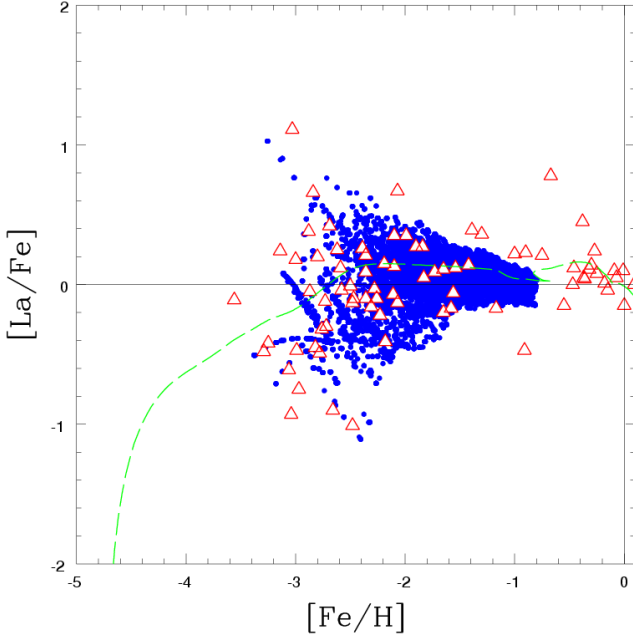


Fig. 4. As in Fig. 2, but for $[\text{La}/\text{Fe}]$. The authors of the observational data are listed in Table 1. The dashed line is the prediction of the homogeneous model (Cescutti et al. 2007a).

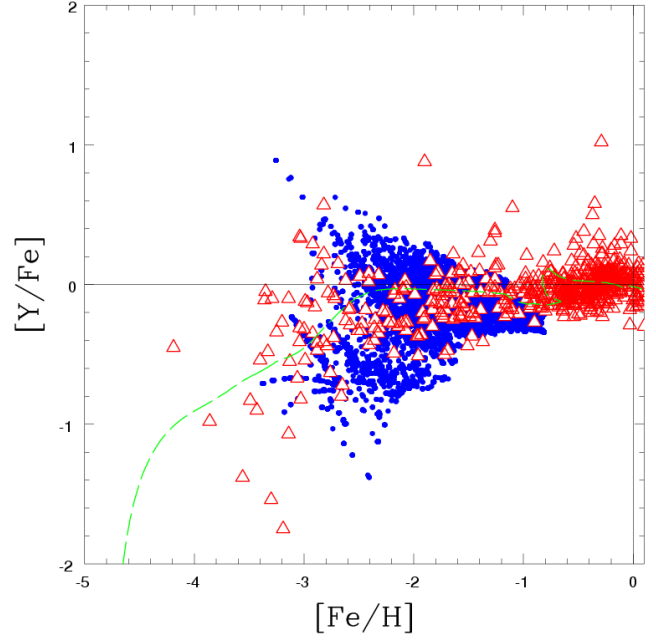


Fig. 6. As in Fig. 2, but for $[\text{Y}/\text{Fe}]$. The authors of the observational data are listed in Table 1. The dashed line is the prediction of the homogeneous model (Cescutti 2007b).

overly rapid rise of $[\text{Fe}/\text{H}]$, related to the adopted infall rate. Indeed, numerical simulations (Recchi et al. 2001) show that the mixing timescale of the ejecta, although fast, is of the order

of 10Myr, therefore larger than the assumed timestep. If included, this delayed mixing might increase the amount of very metal-poor stars. Moreover, the model predicts that $\sim 5\%$ of the simulated stars are metal free. This is the fraction of stars

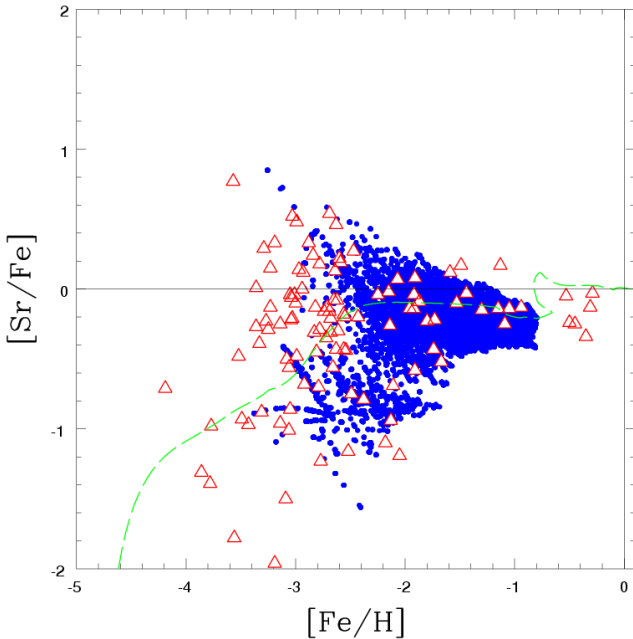


Fig. 5. As in Fig. 2, but for $[\text{Sr}/\text{Fe}]$. The authors of the observational data are listed in Table 1. The dashed line is the prediction of the homogeneous model (Cescutti 2007b).

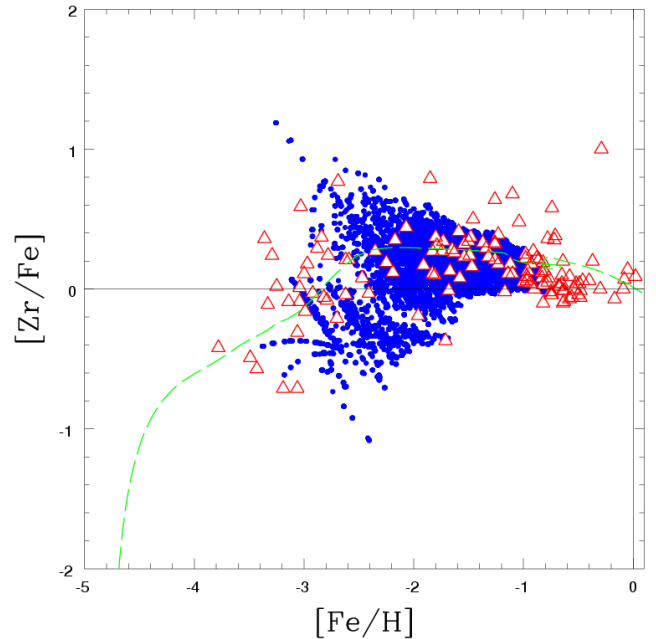


Fig. 7. As in Fig. 2, but for $[\text{Zr}/\text{Fe}]$. The authors of the observational data are listed in Table 1. The dashed line is the prediction of the homogeneous model (Cescutti 2007b).

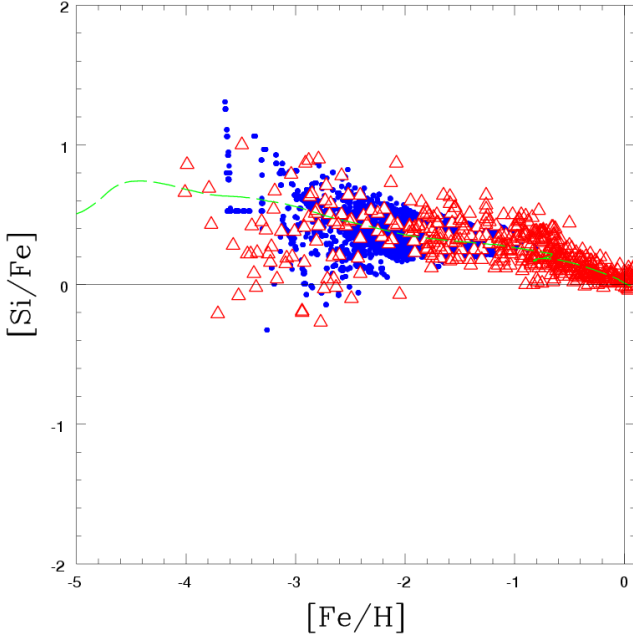


Fig. 8. As in Fig. 2, but for [Si/Fe]. The authors of the observational data are listed in Table 1. The dashed line is the prediction of the homogeneous model (François et al. 2004).

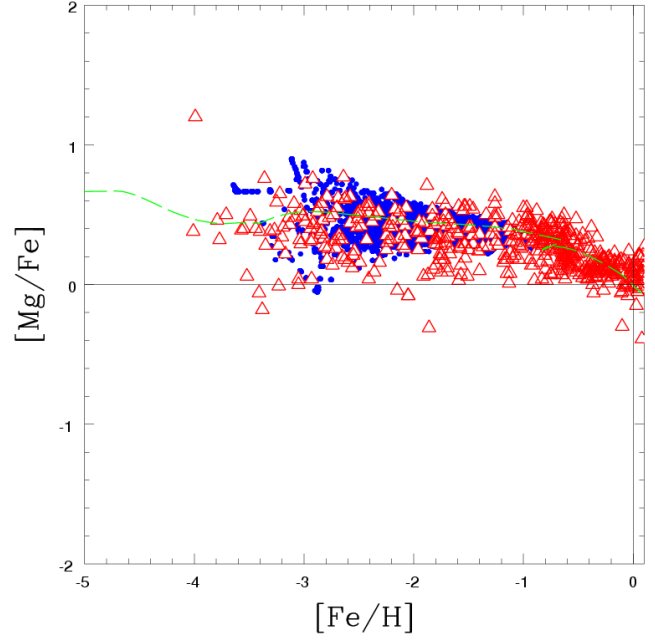


Fig. 10. As in Fig. 2, but for [Mg/Fe]. The authors of the observational data are listed in Table 1. The dashed line is the prediction of the homogeneous model (François et al. 2004).

formed in the first 5 Myr, in which no SN has yet exploded and enriched the ISM. We emphasize that the star formation can be slowed down, for example, by assuming a different infall rate

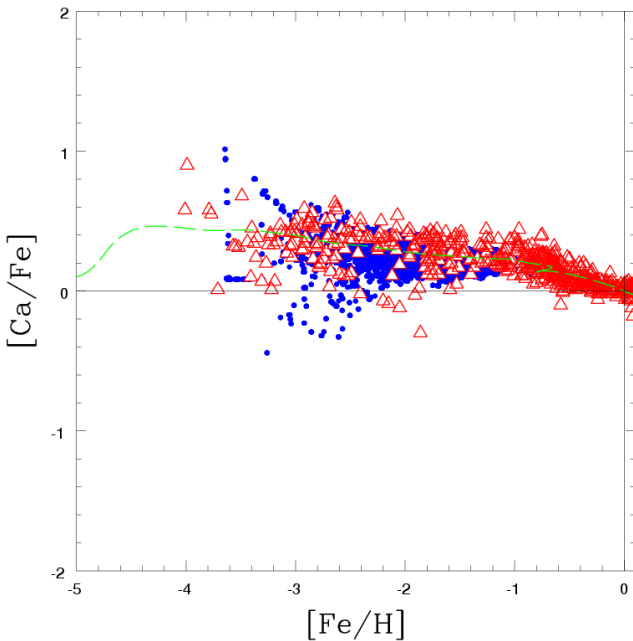


Fig. 9. As in Fig. 2, but for [Ca/Fe]. The authors of the observational data are listed in Table 1. The dashed line is the prediction of the homogeneous model (François et al. 2004).

or a strong outflow of gas from the halo, as recently adopted by Goswami & Prantzos (2000), which would modulate a different star formation. This can solve the absence of ultra metal-poor stars and the too large fraction of metal free stars. The problem of the metal free stars can be also solved by adopting a different IMF. The results of many works (see Larson 1998; Abel, Bryan, & Norman 2000; Hernandez & Ferrara 2001; Nakamura & Umemura 2001; and Mackey, Bromm, & Hernquist 2003) predict that stars formed in a metal free gas must be massive stars. The long-living stars, which are low mass stars, start to form when the ISM has been already enriched by these massive and metal free stars, the so-called Population III. The effect of the Pop III on the global chemical evolution should be negligible (see Matteucci & Pipino 2005, Matteucci & Calura 2005), as it involves a small total amount of recycled mass. In fact, we tested a model with a top-heavy IMF, for the very first period, up to a metallicity $Z = 10^{-4}Z_{\odot}$; we decided to use this value because in the literature $10^{-4}Z_{\odot}$ is considered the metallicity of the transition to have a normal IMF (see Schneider et al. 2002). This stage lasts only about 5-10 Myr, depending on the chosen cubic region. This top-heavy IMF has the same shape of the one we normally use (Scalo et al. 1986), but we changed the lower limit from $0.1M_{\odot}$ to $1M_{\odot}$. We found, in this way, that the chemical evolution does not change but we eliminated the presence of metal-free stars, which are not observed. In fact all the stars, born during this stage will die before the present time and the stars born after will not be metal-free. We emphasize that we have decided to use the same parameters and conditions of the homogeneous model to test the validity of the inhomogeneous one. It is clear from the Figs. that this new model for a high number of star formation events well approximates the ho-

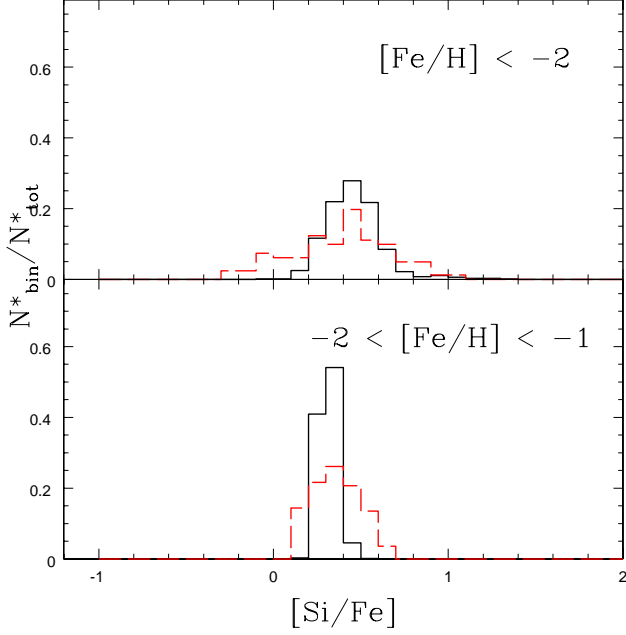


Fig. 11. The relative frequency of stars at a given $[\text{Si}/\text{Fe}]$ ratio for different enrichment phases. In solid line the predictions of the model for the living stars at the present time, in dashed line the observational data. The authors of the observational data are listed in Table 1.

homogeneous model, which is shown by the dashed line in Figs. 2-10.

5.2. The ratios $[\text{Ba}/\text{Eu}]$ and $[\text{Ba}/\text{Y}]$

Our model predicts a spread in the abundance ratios of two elements if the sites of production of these two elements are different, or if the ratio of the yields of these same elements presents large variations as a function of the stellar mass.

This is not the case for the yields of neutron capture elements. In Fig. 13 we show the ratio $[\text{Ba}/\text{Eu}]$ versus $[\text{Fe}/\text{H}]$. As expected, the results of the model shows a small spread, as for the plot of $[\alpha/\text{Fe}]$, being the ratio between the newly-produced Ba and the newly-produced Eu almost constant as a function of the stellar mass. On the other hand, the observational data show a spread larger than predicted in the metallicity range $-2 < [\text{Fe}/\text{H}] < -1$. We observe that most of the data seem to have a larger overabundance of Ba than that predicted by our model. Taking into account this fact, the observational spread could be explained either by an earlier production of Ba by s-process in intermediate stars from 3 to $8M_{\odot}$ (that we do not take in account in our nucleosynthesis); by self enrichment of the observed stars due to dredge-up; or, to a binary system with mass transfer from an AGB star, which is not shining anymore, to the presently observed companion star (see Aoki et al. 2006).

In Fig. 14, we show the ratio $[\text{Ba}/\text{Y}]$ versus $[\text{Fe}/\text{H}]$. The results of the model relative to this ratio are not satisfactory. The observational data show a very large scatter at $[\text{Fe}/\text{H}] \sim -3$ that is not predicted by our model. Contrary to the $[\text{Ba}/\text{Eu}]$

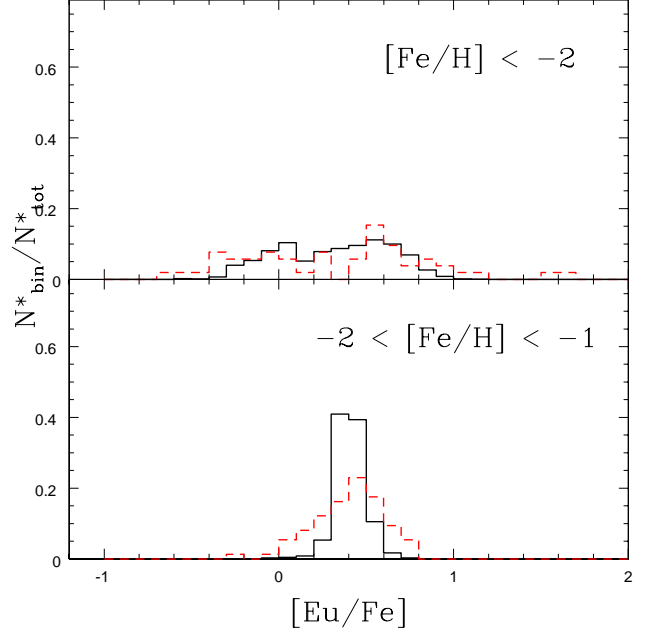


Fig. 12. As in Fig. 11, but for $[\text{Eu}/\text{Fe}]$. The authors of the observational data are listed in Table 1.

ratio, for which the available data show a moderate spread at $[\text{Fe}/\text{H}] \sim -3$, $[\text{Ba}/\text{Y}]$ ratio shows a large spread. One possible explanation for this spread could be that the r-process yields that we use in our model are indicative of the mean contribution by r-process to the abundances of these elements. We emphasize that these two elements are in different peaks in the solar abundances, both for what concern s-process (not so important at this stage) and for what concern r-process. It could be that, as introduced by Otsuki et al. (2003), the r-process is not unique but consists of different contributions and what we use are only the mean values. Massive stars may produce r-process with different patterns, probably as a function of the multiple factors that influence r-process. In our inhomogeneous model, we use only one pattern for all the neutron capture elements. This could be the reason why we are not able to reproduce the spread for the ratios of neutron capture elements. Moreover, this problem should be more visible when we compare neutron capture elements belonging to different peaks as in the case of $[\text{Ba}/\text{Y}]$.

6. Conclusions

In this paper, we tried to solve the problem of the large spread observed at low metallicity of the $[\text{el}/\text{Fe}]$ ratios for neutron capture elements and, at the same time, the smaller spread observed in $[\alpha/\text{Fe}]$ ratios. We developed a new model for the chemical evolution of the halo of the Milky Way. In this model, we coupled the birth of stars with random masses, with different mass ranges for the production of α -elements and neutron capture elements. In particular, the site of production of α -elements is the whole range of the massive stars, from 10 to $80M_{\odot}$ whereas the mass range of production for neutron cap-

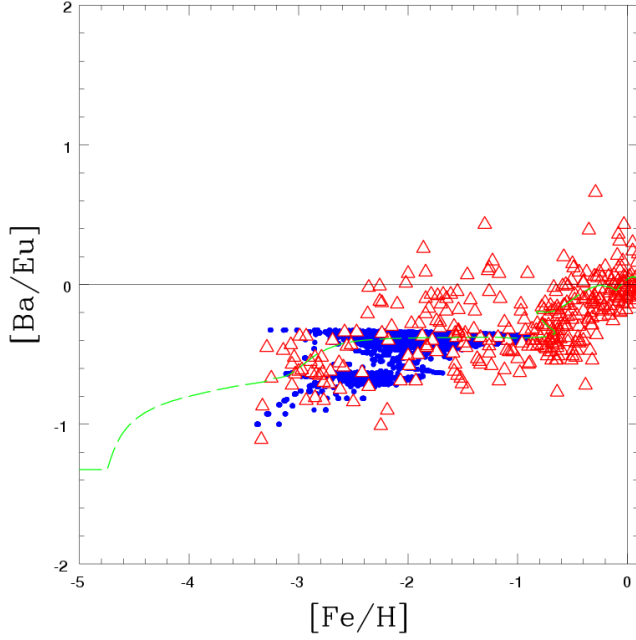


Fig. 13. [Ba/Eu] vs [Fe/H]. The abundances of simulated living stars at the present time in blue dots, the red triangles are the observational data from Burris et al.(2000); François et al. (2007); Fulbright (2000, 2002); Gilroy et al. (1998); Gratton & Sneden (1994); Honda et al. (2004); Ishimaru et al. (2004); Johnson (2002); Mashonkina & Gehren (2000, 2001); McWilliam et al. (1995); McWilliam & Rich (1994); Prochaska et al. (2000); Ryan et al. (1991, 1996); Stephens (1999); and Stephens & Boesgaard (2002). The dashed line is the prediction of the homogeneous model (Cescutti et al. 2006, model 1).

ture elements lies between 12 and $30M_{\odot}$. We showed that these two assumptions can explain the larger spread in the abundances of metal-poor stars for neutron capture elements and the smaller spread for α -elements. We note that the idea of a small range of the r-elements progenitors, as explanation of the large scatter, is not new, having been already proposed by Ishimaru & Wanajo (1999) and Argast et al. (2000), although the mass ranges and the mass dependences of their yields and this work are different. We emphasized that the parameters we used (described in Sect. 3) are the same as the homogeneous model (see Cescutti et al. 2006). We adopted this point of view because these parameters have been already constrained to give good results compared to the observational data at higher metallicities and compared to the mean trends. In fact, toward high metallicities ($[Fe/H] > -2.0$ dex) the model naturally gives results compatible to the homogeneous model. However, this set of parameters is a starting point and the model still needs a better investigation of the parameter space. In particular, concerning the early galactic stages, the model is not able to reproduce ultra metal-poor stars, even though stars with this metallicity are observed. This may be due to an overly rapid rise of $[Fe/H]$, related to the used infall law. To avoid these problems, a different infall law can be used or an outflow from the halo

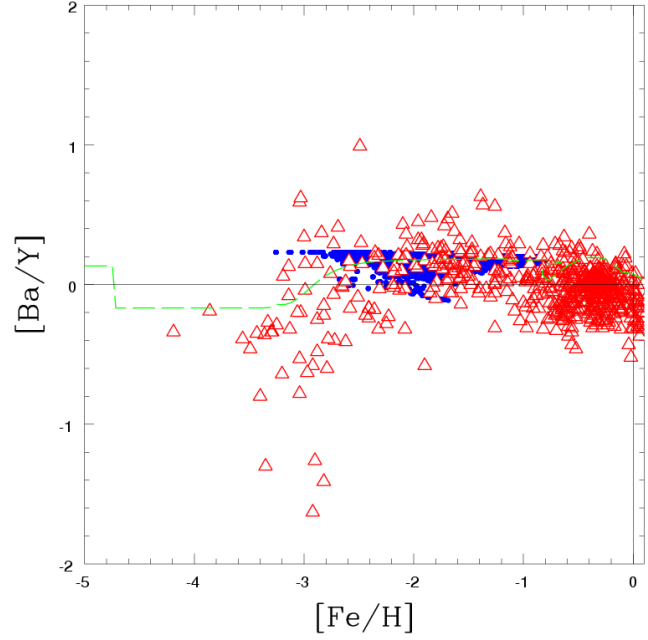


Fig. 14. As in Fig. 13 but for [Ba/Y] vs [Fe/H]. The data for this elements are from Burris et al.(2000); François et al. (2007); Fulbright (2000, 2002); Gilroy et al. (1998); Gratton & Sneden (1994); Honda et al. (2004); Ishimaru et al. (2004); Johnson (2002); McWilliam et al. (1995); McWilliam & Rich (1994); Nissen & Schuster (1997); Prochaska et al. (2000); and Ryan et al. (1991, 1996). The dashed line is the prediction of the homogeneous model (Cescutti 2007b).

can be included to provide a smoother increase of the metallicity. Moreover, this new model generates an over abundance of metal free stars if we do not impose at least a slightly different IMF for the first episodes of stars formation to solve the problem of the metal free stars.

Acknowledgements. GC would like to thank Francesca Matteucci, Patrick François, Francesco Calura, Simone Recchi, and Antonio Pipino for several fruitful discussions, as well as the anonymous referee for valuable comments. The work was supported by the Italian Ministry for the University and Research (MIUR) under COFIN03 prot.2003028039.

References

- Abel T., Bryan G.L., & Norman M.L. 2000, *ApJ*, 540, 39
- Argast D., Samland M., Gerhard O.E., & Thielemann, F.-K. 2000, *A&A*, 356, 873
- Argast D., Samland M., Thielemann, F.-K., & Gerhard O.E. 2002, *A&A*, 388, 842
- Asplund M., Grevesse N., & Sauval A. J. 2005, *ASPC*, 336, 25A
- Beers T.C., Rossi S., Norris J.E., Ryan S.G., & Shefler T. 1999, *A.J.*, 117, 981
- Burris D.L., Pilachowski C.A., Armandroff T.E., et al. 2000, *ApJ*, 544, 302

- Busso M., Gallino R., Lambert D.L., Travaglio, C., & Smith V.V. 2001, *ApJ*, 557, 802
- Cappellaro E., Evans R., & Turatto M. 1999, *A&A*, 351, 459
- Carretta E., Gratton R.G., & Cohen J.G. 2002, *AJ*, 124, 481
- Carney B.W., Wright J.S., Sneden C., et al. 1997, *A.J.*, 114, 363
- Cayrel R., Depagne E., Spite M., et al. 2004, *A&A*, 416, 1117
- Cescutti G. 2007b, PhD thesis, arXiv, 0708.4163
- Cescutti G., François P., Matteucci F., Cayrel R., & Spite M. 2006, *A&A*, 448, 557
- Cescutti G., Matteucci F., François P., & Chiappini C. 2007a, *A&A*, 462, 943
- Chiappini C., Matteucci F., & Gratton R.G. 1997, *ApJ*, 477, 765
- Chiappini C., Matteucci F., & Romano D. 2001, *ApJ*, 554, 1044
- Cowan J.J., Sneden C., Beers T.C., et al. 2005, *ApJ*, 627, 238
- Edvardsson B., Andersen J., Gustafsson B., et al. 1993, *A&A*, 275, 101
- François P., Depagne E., Hill V., et al. 2007, *A&A*, 476, 935
- François P., Matteucci F., Cayrel R., et al. 2004, *A&A*, 421, 613
- Fulbright J.P. 2000, *AJ*, 120, 1841
- Fulbright J.P. 2002, *AJ*, 123, 404
- Gilroy K.K., Sneden C., Pilachowski C.A., & Cowan J.J. 1988, *ApJ*, 327, 298
- Goswami A., & Prantzos N. 2000, *A&A*, 359, 191
- Gratton R.G., & Sneden C. 1988, *A&A*, 204, 193
- Gratton R.G., & Sneden C. 1994, *A&A*, 287, 927
- Hernandez X., & Ferrara A. 2001, *MNRAS*, 324, 484
- Honda S., Aoki W., Kajino T., et al. 2004, *ApJ*, 607, 474
- Ikuta C., & Arimoto N. 1999, *PASJ*, 51, 459
- Ishimaru Y., & Wanajo S. 1999, *ApJ*, 511L, 33
- Ishimaru Y., Wanajo S., Aoki, W., & Ryan, S.G. 2004, *ApJ*, 600L, 47
- Iwamoto, K., Brachwitz F., Nomoto K., et al. 1999, *ApJS*, 125, 439
- Johnson J.A. 2002, *ApJS*, 139, 219
- Karlsson T., & Gustafsson B. 2005, *A&A*, 436, 879
- Koch A., & Edvardsson B. 2002, *A&A*, 381, 500
- Larson R.B. 1998, *MNRAS*, 301, 569
- Mackey J., Bromm V., & Hernquist L. 2003, *ApJ*, 586, 1
- Maeder A., & Meynet G. 1989, *A&A*, 210, 155
- Mashonkina L., & Gehren T. 2000, *A&A*, 364, 249
- Mashonkina L., & Gehren T. 2001, *A&A*, 376, 232
- Matteucci F., & Calura F. 2005, *MNRAS*, 360, 447
- Matteucci F., & Greggio L. 1986, *A&A*, 154, 279
- Matteucci F., & Pipino A. 2005, *MNRAS*, 357, 489
- McWilliam A., Preston G.W., Sneden C., & Searle L. 1995, *AJ*, 109, 2757
- McWilliam A., & Rich R. M. 1994, *ApJS*, 91, 749
- McWilliam A., & Searle L. 1999, *Ap&SS*, 265, 133
- Nakamura F., & Umemura M. 2001, *ApJ*, 548, 19
- Nissen P.E., & Schuster W.J. 1997, *A&A*, 326, 751
- Nomoto K., Tominaga N., Umeda H., Kobayashi C., & Maeda K. 2006, *Nucl. Phys. A*, 777, 424
- Otsuki, K., Mathews G.J., & Kajino T. 2003, *New A*, 8, 767
- Pompeia L., Barbay B., & Grenon M. 2003, *ApJ*, 592, 1173
- Prochaska J.X., Naumov S.O., Carney B.W., McWilliam A., & Wolfe A.M. 2000, *AJ*, 120, 2513
- Raiteri C.M., Villata M., Gallino R., Busso M., & Cravanzola, A. 1999, *ApJ*, 518, L91
- Recchi S., Matteucci F., & D'Ercole A. 2001, *MNRAS*, 322, 800
- Ryan S., Norris J.E., & Bessel M.S. 1991, *AJ*, 102, 303
- Ryan S., Norris J.E., & Beers T.C. 1996, *ApJ*, 471, 254
- Scalo J.M. 1986, *Fund. Cosmic Phys.*, 11, 1
- Schneider R., Ferrara A., Natarajan P., & Omukai K. 2002, *ApJ*, 571, 30
- Stephens A. 1999, *AJ*, 117, 1771
- Stephens A., & Boesgaard A.M. 2002, *AJ*, 123, 1647
- Thornton K., Gaudlitz M., Janka H.-Th., & Steinmetz M. 1998, *ApJ*, 500, 95
- Travaglio C., Gallino R., Arnone E., et al. 2004, *ApJ*, 601, 864
- Tsujimoto T., Shigeyama T., & Yoshii Y. 1999, *ApJ*, 519L, 63
- Wolf V.M., Tomkin J., & Lambert D.L. 1995, *ApJ*, 453, 660